In-vivo Imaging of Femoral Artery Nitinol Stents for Deformation Analysis

Arundhuti Ganguly, PhD, Jeffrey Simons, PhD, Alex Schneider, MS, Benjamin Keck, MSc, Nathan R. Bennett, MS, Robert J. Herfkens, MD, Sheila M. Coogan, MD, and Rebecca Fahrig, PhD

ABSTRACT

Purpose: The authors have developed a direct method to study femoral artery stent deformations in vivo. A previously described imaging and analysis approach based on a calibrated phantom was used to examine stents in human volunteers treated for atherosclerotic disease. In this pilot study, forces on stents were evaluated under different in-vivo flexion conditions.

Materials and Methods: The optimized imaging protocol for imaging with a C-arm computed tomography system was first verified in an in-vivo porcine stent model. Human data were obtained by imaging 13 consenting volunteers with stents in femoral vessels. The affected leg was imaged in straight and bent positions to observe stent deformations. Semiautomatic software was used to calculate the changes in bending, extension, and torsion on the stents for the two positions.

Results: For the human studies, tension and bending calculation were successful. Bending was found to compress stent lengths by 4% ± 3% (−14.2 to 1.5 mm), increase their average eccentricity by 10% ± 9% (0.12 to −0.16), and change their mean curvature by 27% ± 22% (0 to $-0.005\ mm^{-1}$). Stents with the greatest change in eccentricity and curvature were located behind the knee or in the pelvis. Torsion calculations were difficult because the stents were untethered and are symmetric. In addition, multiple locations in each stent underwent torsional deformations.

Conclusions: The imaging and analysis approach developed based on calibrated in vitro measurements was extended to in-vivo data. Bending and tension forces were successfully evaluated in this pilot study.

There has been an increased interest in understanding the causes of reported fracture of femoral artery stents (1). Several in-vivo studies have examined the deformations of stents in various parts of the body through several indirect approaches. Some studies have used computed tomographic (CT) angiography to measure changes in stent length and vessel lumen sizes (2,3). However, the CT measurements have not been correlated quantitatively with the equivalent distorting forces. In one study (4), x-ray projection images were obtained in cadaveric legs under different bending and flexion conditions. Other studies (5,6) have used magnetic resonance (MR) imaging to investigate the deformation of vessels alone following flexion of various body parts. However, because MR cannot be used to image metallic stents accurately (7), this type of evaluation provides only an indirect indication of the deforming forces on the stent. In addition, these MR studies were performed on young healthy volunteers and might not be representative of the behavior of the vasculature in the elderly population most commonly treated with stents for atherosclerotic disease.

We have developed a more direct approach of studying femoral stent deformations, which involves imaging the stent-implanted leg under different flexion conditions in human subjects previously treated for vascular disease. In an accompanying publication (8), we reported on a phantom-based imaging and image analysis framework for measurement of the deformations of femoral artery stents. After this framework was validated through the in vitro study, the imaging and analysis approach was then used to study stent deformations in human volunteers. By using images obtained from a C-arm CT system, a protocol was developed for imaging stents and analyzing their deformations. This

From the Department of Radiology (A.G., J.S., B.K., R.J.H., R.F.), Stanford University, 1201 Welch Rd., Palo Alto, CA 94305; Veterans Affairs Palo Alto Healthcare System (S.M.C.), Palo Alto; SRI International (A.S., N.R.B.), Menlo Park, California. Received August 23, 2010; final revision received and accepted October 20, 2010. **Address correspondence to** A.G.; E-mail: aganguly@stanford.edu

Present address of B.K.: Pattern Recognition Lab and Medical Image Reconstruction Group, Friedrich-Alexander-Universität Erlangen-Nürnberg, 91054 Erlangen, Germany.

This work was funded by the sponsors of the RESIStent program: Abbott Vascular (Santa Clara, California), Angiomed (Karlsruhe, Germany), Boston Scientific (Natick, Massachusetts), Cordis (Warren, New Jersey), Medtronic (Minneapolis, Minnesota), and W. L. Gore and Associates (Tempe, Arizona).

None of the authors have identified a conflict of interest.

J Vasc Interv Radiol 2011; 22:244–249

DOI: 10.1016/j.jvir.2010.10.019

direct approach may lead to better understanding for the causes of superficial femoral artery stent fracture.

MATERIALS AND METHODS

All imaging was performed on a C-arm CT angiographic/fluoroscopic system (Axiom Artis dTA; Siemens, Forchheim, Germany). Image acquisition and reconstruction parameters described previously (8) were used (96 kVp with automatic exposure control, 20 s rotation, detector pixel size of 154 μm, reconstruction voxel size of 150 μm^3 with 512 × 512 × 512 voxels in the region of interest, and "vessel-sharp" reconstruction kernel).

Animal Imaging

To verify the suitability of the chosen in-vivo stent imaging protocol, a nitinol stent placed in the femoral artery of a swine was imaged with use of the C-arm system. This prospective study was conducted with institutional review board approval. The swine was preanesthetized with a mixture of Telazol (tiletamine HCL and zolazepam HCL) and atropine followed by inhalation of 2%–3% isoflurane. All vital functions of the animal were constantly monitored after induction of anesthesia. The stent was imaged with the stent-implanted leg straight and then bent at the knee and hip.

Human Subject Imaging

A pilot study to evaluate our technique was conducted by imaging 13 subjects who had stents implanted in arteries in the femoral region. The human subjects who participated in the study had previously undergone stent treatment for atherosclerotic disease in the femoral vessels at a collaborating medical facility. Subjects with stents located in any of the vessels in the femoral region were accepted in view of the limited population accessible during the course of the study. Some subjects had been treated with multiple stents, and the stent types and manufacturers varied among and even within subjects. Based on the parameters from the phantom and animal studies, a protocol was developed and approved by an institutional review board at the authors' university. All subjects gave informed consent before imaging. The population statistics of the imaged group are listed in **Table 1**.

For imaging the deformations of superficial femoral artery stents, the subjects were placed in two positions: one with the affected leg straight and the other with the leg bent at the hip, knee, and ankle. A special extension to the existing patient table was constructed to allow placement of the subject in the two positions such that the stent always remained at isocenter during imaging. The distances between the focal spot and center of rotation and between the focal spot and detector, along with subject height, limited how far the subjects could bend their hip and knee while allowing unobstructed rotation of the C-arm. **Figure 1** shows the setup for imaging the subjects with the C-arm system. An angled back support and an ankle support were provided. Further support was provided in the form of adjustable straps. This was necessary to minimize leg movement and/or tremors during the scan to prevent any motion artifact from reducing image quality.

From the image data, the values for the centerline length and the curvature along the centerline were extracted. This allowed for calculations of the response to

Table 1. Statistical Details of Human Subjects Imaged (N = 13)

Detail	Value
Pts. with usable images	11
Sex (M/F)	12 : 1
Age (y)	67 ± 8.5
Height (cm)	176 ± 9
Weight (kg)	88.4 ± 10.9

Note.—Values presented as means ± SD.

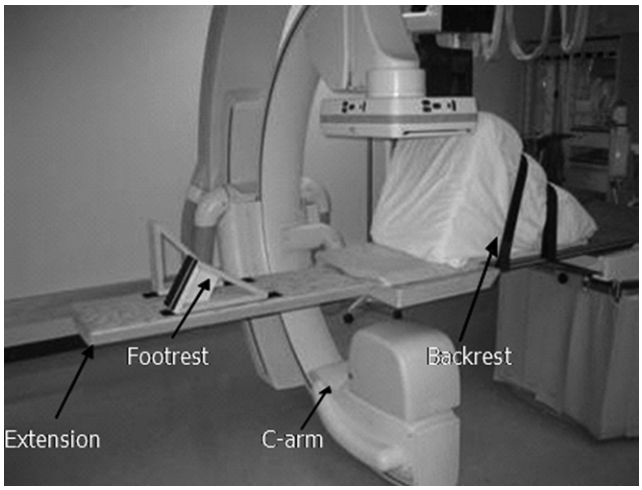

Figure 1. Setup for imaging human subjects with the C-arm system.

Table 2. Imaging Parameters for Study in Human Subjects

Parameter	Value
Scan time, s	20*
Frames per second	15
Frames per scan	494
Peak tube voltage, kVp	90
Focal spot size, mm	0.6
Reconstruction kernel	Bone, sharp
Dose level to detector, μGy	0.120
Detector matrix size	1,024 × 1,024
Reconstruction voxels	512 × 512 × 512
Voxel size, μm	214 ± 66†

* Time for each leg position.
† Region of interest–dependent.

Table 3. Summary of Measurements from Human Subject Imaging Study

	Stent Location	No. of Stents	Stent Length (mm)	Mean Eccentricity	Mean Curvature (l/mm)	Mean Bent Radius (mm)	Min Bent Radius (mm)	Max Bent Radius (mm)
Straight	Mid-thigh	3	95.078	0.45	0.008	127	32	400
Bent			94.133	0.52	0.01	98	20	3333
Straight	Near hip—Groin	1	59.503	0.27	0.026	39	20	89
Bent			59.659	0.34	0.021	48	34	98
Straight	R groin	1	62.841	0.35	0.009	111	57	455
Bent			61.893	0.46	0.015	66	26	714
Straight	R pop A*: behind knee	1	132.983	0.25	0.009	112	66	714
Bent			121.021	0.34	0.025	40	19	185
Straight	L SFA: entire thigh	4	184.126	0.59	0.006	164	43	2000
Bent			169.756	0.42	0.017	39	17	435
Straight	R SFA: mid-thigh	1	43.455	0.38	0.012	80	30	263
Bent			43.163	0.46	0.01	96	47	208
Straight	R SFA: upper thigh/groin	1	64.484	0.33	0.01	100	49	196
Bent			62.143	0.37	0.013	77	40	435
Straight	R SFA: mid-thigh	2	101.051	0.44	0.006	179	35	5000
Bent			95.059	0.45	0.006	175	34	1000
Straight	R SFA: mid-thigh	3	85.836	0.40	0.017	58	17	323
Bent			84.575	0.42	0.014	71	28	385
Straight	L SFA: mid-thigh	2	95.467	0.44	0.007	135	27	3333
Bent			89.478	0.48	0.011	91	19	588
Straight	R SFA: mid-thigh	1	88.939	0.48	0.011	94	33	556
Bent			90.396	0.55	0.01	101	41	1250
Mean straight:		**1.8**	**92.2**	**0.40**	**0.011**	**109**	**37**	**1212**
Mean bent:			**88.3**	**0.44**	**0.014**	**82**	**30**	**785**

Note:—The numbers in bold are the mean values for the two cases analyzed, and they summarize the results. R = right, L = left.
* Pop A = popliteal artery.

tension. The bend angle was calculated by summing the angles between successive centerline points.

RESULTS

The imaging parameter optimization during the animal study resulted in the values listed in **Table 2**, which were selected for the human subject studies. The animal study showed that stent visibility was sufficient for centerline extraction. However, in the animal imaged, the difference in the stent diameter along the length between the straight and bent leg measured from a planar reformatted C-arm CT image was not significant (ie, < 1 pixel).

The reconstruction voxel size depended on the size of the region of interest including the stent; higher resolution is possible for smaller regions of interest because the total number of voxels was fixed at 5,123. The region of interest size ranged from 103 μm to 383 μm depending on the size of the stent-implanted volume and its anatomic location. The mean value of the reconstruction voxel size was 214 μm $\pm$ 66.

The imaging results in 13 subjects are listed in **Table 3**. Image quality was sufficient for analysis in 11 of 13 subjects. In the two cases of unusable images, the location of the bent leg was not optimal, resulting in truncated reconstructions of the stents. A sample three-dimensional image of a subject with the leg placed in straight and bent positions, and the corresponding unwrapped images, are shown in **Figure 2**.

With our image analysis software, the stents were found to compress in length as a result of leg bending by an average of 4% $\pm$ 3%, with a minimum change of 0.3% and a maximum change of 9.0% (12 mm in a stent-implanted vessel of 133 mm). In four subjects, the change in length was less than 1 mm, with no correlation between number of stents and length change. One subject showed an increase in length of 1.6%, or 1.5 mm in an 89-mm stent. Eccentricity averaged over the length of the stents in straight position was 0.40, compared with 0.44 in the bent position. This represents a 10% increase in eccentricity between the straight and bent positions on average. The maximum deformation of 36% occurred in cases in which the stent was located in the pelvis or behind the knee. A similar pattern was seen for curvature, with only two stents, one in the pelvis and the one behind the knee, exhibiting a significant change in curvature ($P < .01$). The mean curvature mea-

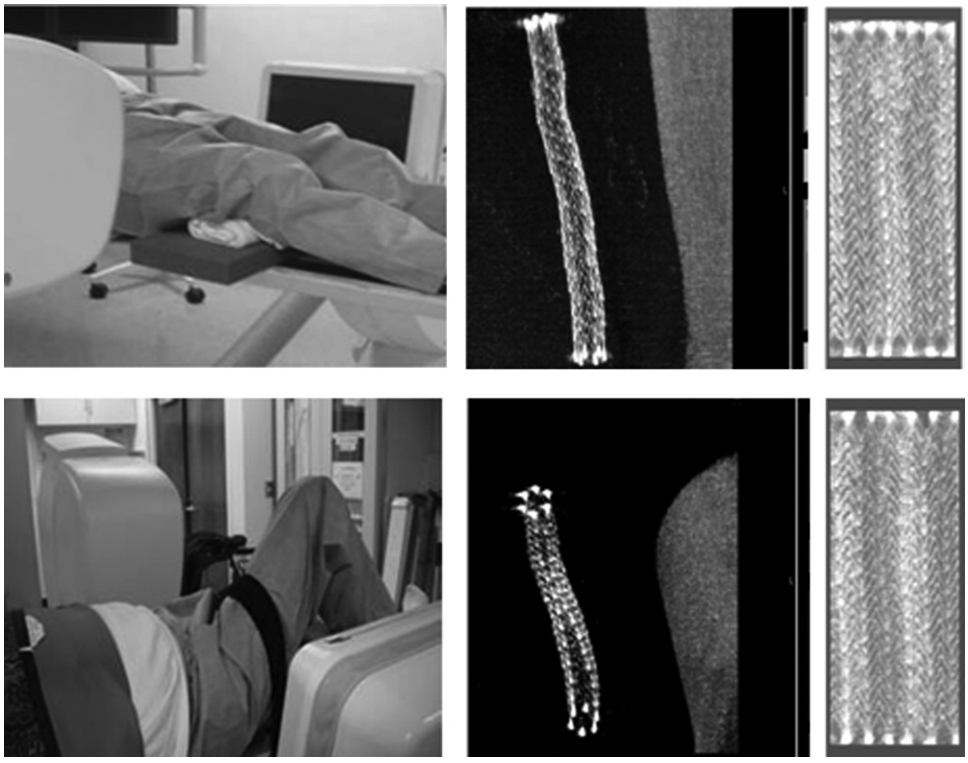

Figure 2. Imaging of a subject with superficial femoral artery stents with the C-arm CT system with the leg in straight (top) and bent (bottom) positions. The corresponding three-dimensional reconstructed images of the stent and the two-dimensional unwrapped stent images are also shown.

surements for straight and bent positions were 0.011 and 0.014, respectively, or a change of 27% ± 22%. **Figure 3** shows the case with the highest degree of curvature. The presence of multiple stents in some of the subjects was ignored for this feasibility study. However, it can have an impact on the results and needs to be studied more carefully.

According to the results from the image-based in vitro measurements, the maximum change in length of the stent of 12 mm corresponds to a load of 466.6*g*. This was obtained by using a linear fit to the theoretical curve for load tension. From the curvature results, the maximum curvature value of 0.054 corresponds to a bend angle of 100.9° or a load of 86.7*g*. The torsion values were not calculated for the human subject data because, in many cases, there were multiple points under torsion.

DISCUSSION

This work provides an estimate of the in-vivo deformation of femoral stents in live subjects. It lays a foundation for an expanded study that could then be used to possibly improve stent design. Additionally, the subjects imaged for this study had received stents with a variety of sizes and lengths and, in many cases, multiple stents from different manufacturers were implanted during their treatment. The locations of the stents in the subjects were variable and the total number of participants in the study was small. This makes extension of the in-vitro results to the in-vivo data less straightforward.

The image analysis algorithm required adjustment of some of the initial conditions. A good estimation of the radius of the stent and the initial direction vector for the centerline was needed. The radius was determined by looking at the cross-sectional slices and manually measuring the stent diameter from a slice in which the stent was fairly rounded. The initial vector was estimated from the orientation of the stent in the volume and was adjusted by trial and error in cases in which the centerline veered off in an obviously incorrect direction. This problem occurred more often when the stent was close to the femur. Another parameter that sometimes needed adjustment was the step size for the centerline calculation. Large step size caused the centerline to hit the wall of the stent in cases in which there was any significant change in curvature. Too small a step size often caused the analysis to be stuck at certain locations. Therefore, in each case, the analysis was started with use of the largest step size and then reduced in case the centerline did not reach the other end of the stent. For the tension measurements, as the results primarily depend on the length change measurements, any error is attributed to inaccuracies in the stent end determination resulting in errors in the calculated stent length.

For torsion calculations, given the image resolution, the relative shift in the location of stent wires at locations

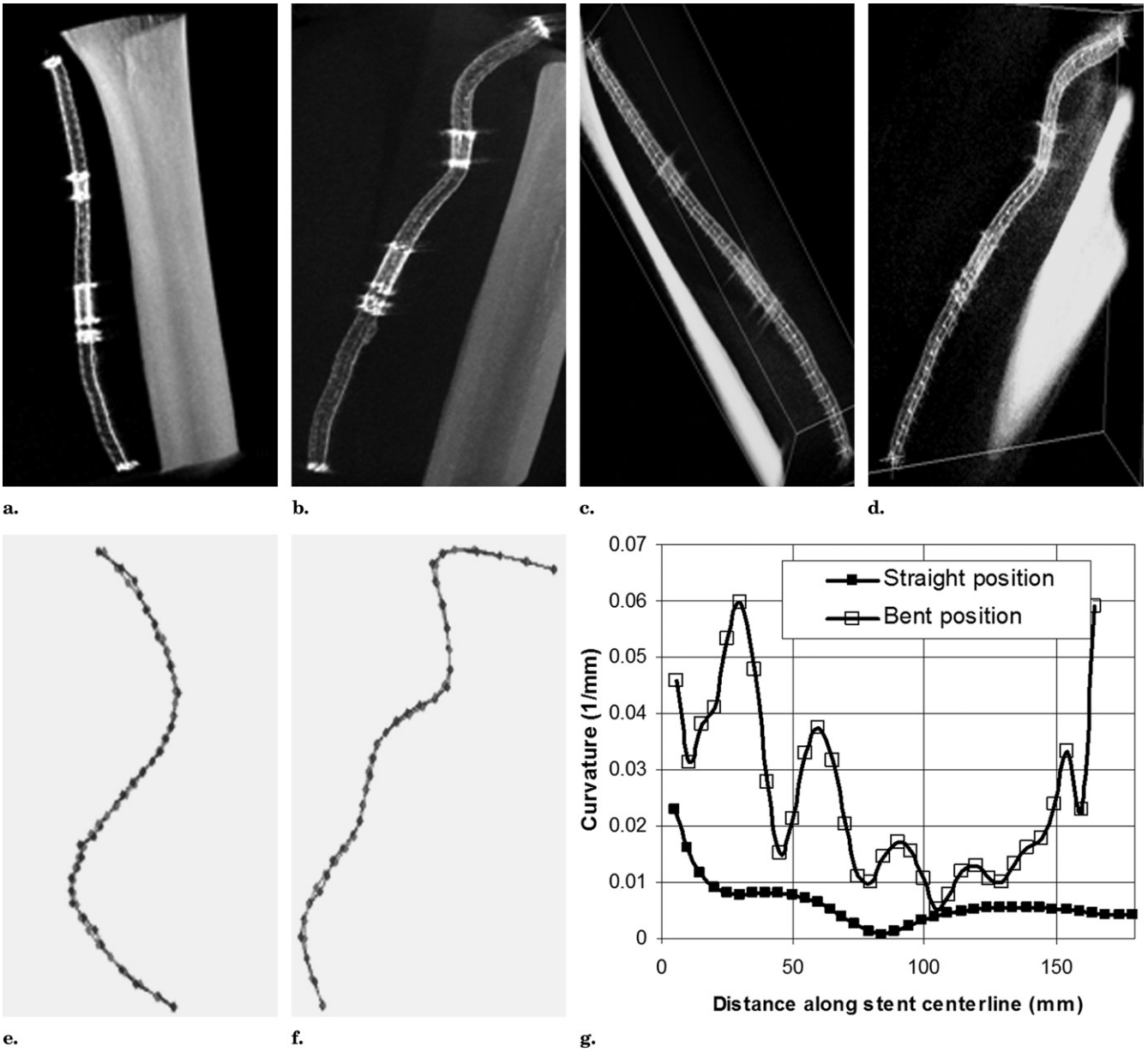

Figure 3. Three-dimensional stent images for a subject with the leg in straight **(a)** and bent **(b)** positions and corresponding images with overlaid centerline **(c,d)**. Corresponding fits to three-dimensional centerline using polynomial fit (grey) **(e,f)** and calculated curvature **(g)** for the two positions.

other than near the gold markers was difficult to identify accurately. In the in vitro setup, it was assumed that one end of the stent was fixed and torque was applied to the other end; hence, the effect of torque could be quantified. In the human subjects, the stents were not tethered at either end, which made the torsion calculations difficult. The circular symmetry of the stents made the torque calculations from the unwrapped stent even more difficult. Additional work involving connected graphs and use of calcification as markers in the vicinity of the stents is under way (9).

Analysis of the results showed significant noise in the eccentricity along the length of the stent. Although some of the variations reflect the actual physical condition, a major contributor to this result is the presence of high-density plaque around the stent. **Figure 4** shows two cases in which the plaque was most significant. The analysis software is unable to distinguish between the stent wires and the plaque, which causes inaccurate ellipses to be fitted perpendicular to the centerline. A possible solution to this issue could be to obtain images before the procedure that could then be registered and subtracted from the images with the stents in place to numerically remove the plaque from the three-dimensional images before stent analysis.

Comparing our measurements versus in-vivo measurements in the literature, CT angiographic studies report stent dimensions with length measurement accuracies of 2.46 mm ± 2.37 for cardiac stents (3) and 1.9–0.94 mm for lumen diameters of vertebral artery stents (2). Although the

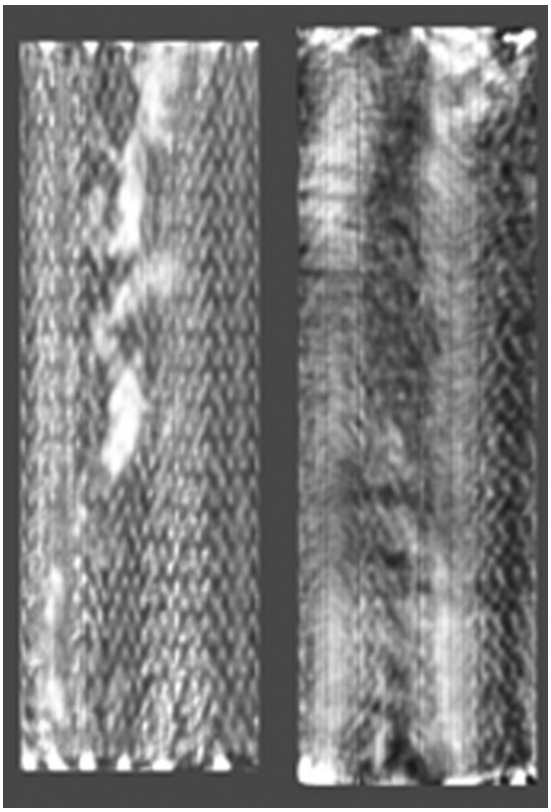

Figure 4. Unwrapped stent images show deposited plaque.

errors in stent length measurements for our previous in vitro studies averaged 0.7 mm ± 0.5 (8), this could not be calculated for the in-vivo study. The primary reason was the unavailability of the physical measurement of the length of the deployed stent or of the multiple overlapping stents used in many cases. We did not record the stent diameter because the value was not needed directly for our calculations. However, the cross-sectional boundary was identified by the algorithm and used for calculation of the centerline, which was then used to calculate the tension and bending.

A fairly recent study by Nikanorov et al (4) looked at projection x-ray images of stents placed in cadaveric legs and estimated the compression and deflection or bend angle. The maximum axial compression was 11%. In comparison, the maximum compression in our subjects was 36%. In the study of Nikanorov et al (4), the stents were then placed inside silicone tubing and subjected to 10 million cycles of chronic fatigue testing. Chronic compression of 5% could result in a fracture rate as high 80%, and a bend angle of 48° could result in an almost 100% fracture rate in some stents. Although the subjects in the present study did not exhibit any stent fracture, some experienced high compression and large bend angles as reported earlier.

In summary, an imaging and image-analysis technique for the study of deformations of femoral artery stents has been tested in an in-vivo pilot study. From this study, we realized that the range of loads studied in the in vitro experiment must be increased to span the full physiologic range, and should also include more stent designs to provide a broader reference dataset. Including weight-bearing positions of the leg for the in-vivo studies would increase insight into the causes of stent fracture. More flexible trajectories of the C-arm that have recently been made possible in these scanners would indeed permit imaging such positions. Even though the current study lacks some degree of completeness, it lays the basic groundwork and provides some important initial results.

ACKNOWLEDGMENTS

The authors thank Doug Schwandt for designing and constructing the patient support structures for use during x-ray imaging.

REFERENCES

1. Pelton AR, Schroeder V, Mitchell MR, Gong XY, Barney M, Robertson SW. Fatigue and durability of Nitinol stents. J Mech Behav Biomed Mater 2008; 1:153–164.
2. Maintz D, Seifarth H, Raupach R, et al. 64-slice multidetector coronary CT angiography: in vitro evaluation of 68 different stents. Eur Radiol 2006; 16:818–826.
3. Yoo WJ, Lim YS, Ahn KJ, Choi BG, Kim JY, Kim SH. Assessment of vertebral artery stents using 16-slice multi-detector row CT angiography in vivo evaluation: comparison of a medium-smooth kernel and a sharp kernel. Eur J Radiol 2009; 70:362–368.
4. Nikanorov A, Smouse HB, Osman K, Bialas M, Shrivastava S, Schwartz LB. Fracture of self-expanding nitinol stents stressed in vitro under simulated intravascular conditions. J Vasc Surg 2008; 48:435–440.
5. Brown R, Nguyen TD, Spincemaille P, Prince MR, Wang Y. In vivo quantification of femoral-popliteal compression during isometric thigh contraction: Assessment using MR angiography. J Magn Reson Imaging 2009; 29:1116–1124.
6. Choi G, Shin LK, Taylor CA, Cheng CP. In vivo deformation of the human abdominal aorta and common iliac arteries with hip and knee flexion: implications for the design of stent-grafts. J Endovasc Ther 2009; 16:531–538.
7. Maintz D, Kugel H, Schellhammer F, Landwehr P. In vitro evaluation of intravascular stent artifacts in three-dimensional MR angiography. Invest Radiol 2001; 36:218–224.
8. Ganguly A, Simon J, Schneider A, et al. In vitro imaging of femoral artery nitinol stents for deformation analysis. J Vasc Interv Radiol 2011; 22:236–243.
9. Keck B. A framework for extraction of stent deformation. Thesis. Friedrich-Alexander-Universitat Erlangen-Nurnberg, Nuremberg, Germany, 2007.